

Electronic Supplementary Information for

Two-electron-active Tetracyanoethylene for Nonaqueous Redox Flow Batteries

Xiao Wang,^{a,#} Jingchao Chai,^{a,#} Nilakshi Devi,^a Amir Lashgari,^a Ashwin Chaturvedi,^a Jianbing

“Jimmy” Jiang^{a,*}

^aDepartment of Chemistry, University of Cincinnati, P.O. Box 210172, Cincinnati, Ohio 45221-0172, United States

*Corresponding author: jianbing.jiang@uc.edu

#Equal contribution

Table of Content

Contents	Page
Experimental section	S2–S3
Figure S1. Photograph of 2.0 M TCNE in MeCN.	S4
Figure S2. Cyclic voltammograms of 5.0 mM TCNE in 0.1 M NaClO ₄ /MeCN and 0.1 M TBAPF ₆ /MeCN.	S4
Figure S3. Electrostatic potential map of TCNE at the neutral and reduced states.	S4
Figure S4. Cyclic voltammograms of 5.0 mM TCNE in different voltage range at the scan rate from 5 to 2000 mV/s.	S5
Figure S5. Koutecký-Levich curve (current ¹ vs. $\omega^{-1/2}$) at different reduction overpotentials of the second reduction of TCNE.	S5
Figure S6 Kinetic properties of PEG1-PTZ.	S6
Figure S7. Schematic for static batteries.	S7
Figure S8. The battery performance of 0.2 M static battery.	S7
Figure S9. Nyquist impedance of the 0.5 M static TCNE/PEG1-PTZ battery before and after cycling.	S8
Figure S10. Cyclic voltammograms of 0.2 M TCNE/PEG1-PTZ flow battery before and after cycling.	S8
Figure S11. Nyquist impedance of the TCNE/PEG1-PTZ battery at 20%, 40%, 60%, 80% and 100% state-of-charge.	S9
Figure S12. High-frequency ASR, and polarization ASR of the battery vs. the state-of-charge.	S9
References	S11

Experimental section

1 Chemicals and manipulations

All chemicals were purchased from Sigma-Aldrich, stored in an argon-filled glovebox, and used as received. The NMR analysis was performed at room temperature using a Bruker AV 400 MHz spectrometer. Compound **PEG1-PTZ** was prepared according to a reported procedure.^{S1}

2. Cyclic Voltammetry Studies

A glassy carbon with a diameter of 3.0 mm was used as the working electrode, which was polished with 50 nm Al₂O₃. Platinum wire (0.5 mm) and Ag/AgNO₃ electrode were used as the counter and reference electrodes, respectively. All experiments were conducted in a three-neck flask in an argon-filled glovebox. All cyclic voltammograms were collected with a Bio-Logic potentiostat at a scan rate of 50 mV/s using 5.0 mM active materials in 0.1 M NaClO₄/MeCN solution.

3. Calculation of diffusion coefficient and electron transfer rate constants.

The diffusion coefficient (D) of TCNE was calculated from the Randles-Sevcik equation below:

$$i_p = 0.4463nFAC \left(\frac{nFDv}{RT} \right)^{1/2} \quad \text{Equation S1}$$

Where i_p is reduction peak current (A), n is the number of electrons in the redox process ($n = 1$ or 2), F is Faraday's constant (96,485 C/mol), A is the area of the glassy carbon electrode (0.071 cm²), D is the diffusion coefficient (cm²/s), C is concentration of TCNE (5×10^{-6} mol/mL), v is the scan rate (V/s), R is the universal gas constant (8.314 J K⁻¹ mol⁻¹), and T is the absolute temperature (298 K).

Linear sweep voltammetry (LSV) measurements were carried out using an electrochemical working station (CHI-760e, Chenhua) with a RED (glassy carbon, 5.0 mm in diameter, PINE) as the working electrode. A Ag/AgNO₃ reference electrode and platinum wire were used as the reference and counter electrodes, respectively. A solution of 1.0 mM TCNE or **PEG1-PTZ** in 0.1 M NaClO₄/MeCN was purged with argon for 10 mins to remove dissolved O₂. RED was rotated from 100 rpm to 2500 rpm and the voltage was conducted by sweeping from 0.5 to -2.2 V vs. Ag/Ag⁺. The diffusion coefficients are calculated according to the Levich equation below:

$$i_L = 0.620nFAD^{2/3}C_0\omega^{1/2}\nu^{-1/6} \quad \text{Equation S2}$$

Where i_L is limiting current density (A), n is the number of electrons in redox process ($n = 1$ or 2), F is Faraday's constant (96,485 C/mol), A is the area of the glassy carbon electrode (0.196 cm²), C_0 is the concentration of TCNE (1×10^{-6} mol/cm³), ω is angular rotation rate (rad/s) and ν is the kinematic viscosity of 0.1 M NaClO₄/MeCN (0.004809 cm²/s).^{S2} The kinetic rate constant is calculated according to Equation S3 below:

$$i_0 = FAC_0k_0 \quad \text{Equation S3}$$

Where i_0 was calculated from fitting line of Butler-Volmer equation, x-intercept is the log of the exchange current i_0 , F is Faraday's constant, A is the area of the glassy carbon electrode

(0.196 cm²), C_0 is the concentration of **TCNE** (1×10^{-6} mol/cm³), k_0 is reaction rate constant (cm/s).

The theoretical energy density of the **TCNE** battery was calculated according to Equation S4,^{S3} where n is the number of electrons involved in the cell reaction, C is the concentration of active materials, F is Faraday's constant, V is the cell voltage, and μ is the factor that represents the overall volumes of anolyte and catholyte ($\mu = 1 + (\text{max solubility; less soluble electrolyte})/(\text{max solubility; more soluble electrolyte})$):

$$\text{Energy density (Wh/L)} = nCFV/\mu \quad \text{Equation S4}$$

4. Battery measurements

A RFB device was composed of aluminum alloy plate, polytetrafluoroethylene plate, copper plate, graphite current collector, polytetrafluoroethylene frame, and graphite felt electrodes with an active area of 5 cm². Daramic[®] 175 membrane or Celgard[®] PP 2325 was sandwiched between two graphite felts without pretreatment. All battery measurements were conducted on a Bio-Logic VSP potentiostat. For the 0.2 M-**TCNE** static battery, 0.2 M **TCNE** and 0.48 M **PEG1-PTZ** in 0.5 M NaClO₄/MeCN (1.0 mL) was used as anolyte and catholyte, respectively. For the 0.5 M-**TCNE** static battery, 0.5 M **TCNE** and 1.2 M **PEG1-PTZ** in 1.2 M NaClO₄/MeCN (1.0 mL) was used. For both static battery tests, Celgard[®] PP 2325 was sandwiched between two graphite felts as the separator. For 0.2 M-**TCNE** flow battery, mixed 0.2 M **TCNE** and 0.48 M **PEG1-PTZ** in 1.2 M NaClO₄/MeCN (3.5 mL) was used. For 0.5 M-**TCNE** flow battery, mixed 0.5 M **TCNE** and 1.2 M **PEG1-PTZ** in 1.2 M NaClO₄/MeCN (3.5 mL) were used. For both flow battery tests, Daramic[®] 175 membrane was sandwiched between two graphite felts as the separator. For a flow battery setup, the thicker Daramic[®] 175 separator present better performance on mitigating crossover due to the longer channel for the redox-active species to pass through. In addition, the relatively high mechanical strength of Daramic[®] 175 could withstand the impact of the flowing liquid better. While for a static battery setup, without the concerns of strong crossover effect and liquid flow impact, the Celgard[®] PP 2325 membrane lower-impedance becomes a better choice.

Polarization curves of full battery at different SOCs were recorded following the procedure below: The battery was charged and discharged 3 cycles at first, followed by being charged to the desired SOC and then polarized by LSV at a scan rate of 100 mV/s and a voltage range of -0.4 to 2.2 V.

The impedance of the battery was measured via electrochemical impedance spectroscopy with a frequency range from 100 mHz to 1.0 MHz.

5. Calculation Method

All calculations were carried out by using Gaussian 09^{S4} software for natural, one and two-electron reduction states. All oxidation states were optimized at ground states with density functional theory and (DFT) B3LYP/6-311+G basis sets. Furthermore, restricted (spin unpolarised) DFT model was used for **TCNE** and **TCNE**²⁻, while spin polarised Kohn-Sham DFT (unrestricted) calculation was performed for **TCNE**⁻. The polarizable continuum model was selected to optimize all geometries in acetonitrile to include the solvation effect to the free energies. The molecular orbitals and electrostatic potential calculations were carried out with DFT method at B3LYP/6-311+G level.



Figure S1. Photograph of 2.0 M TCNE in MeCN.

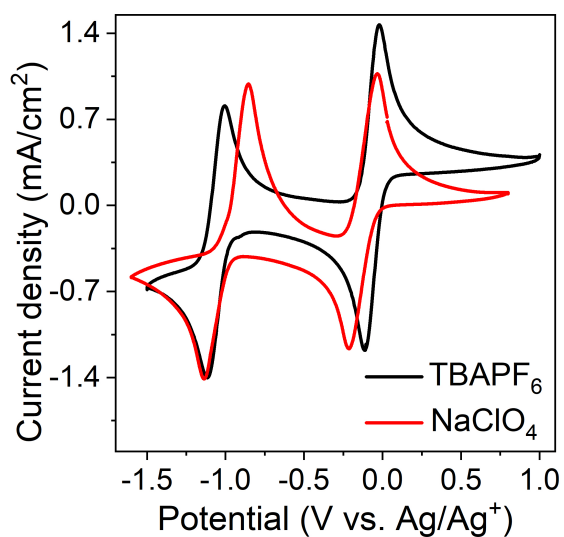


Figure S2. Cyclic voltammograms of 5.0 mM TCNE in 0.1 M NaClO₄/MeCN and 0.1 M TBAPF₆/MeCN at a scan of 50 mV/s.

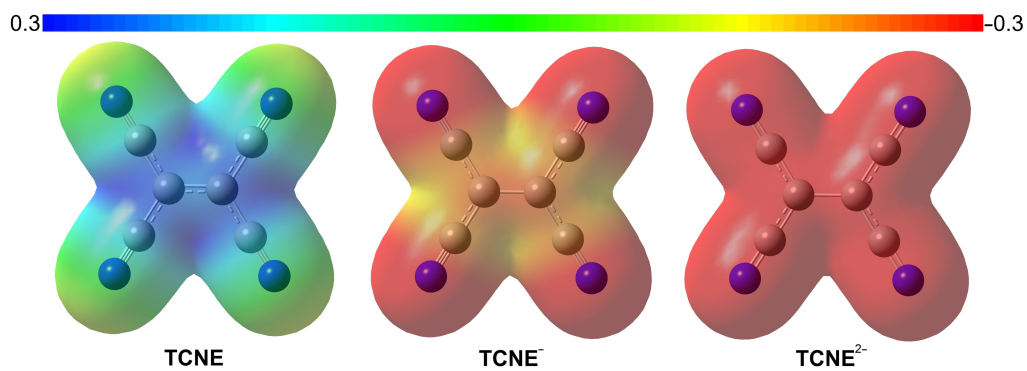


Figure S3. Electrostatic potential map of TCNE at the neutral reduced states.

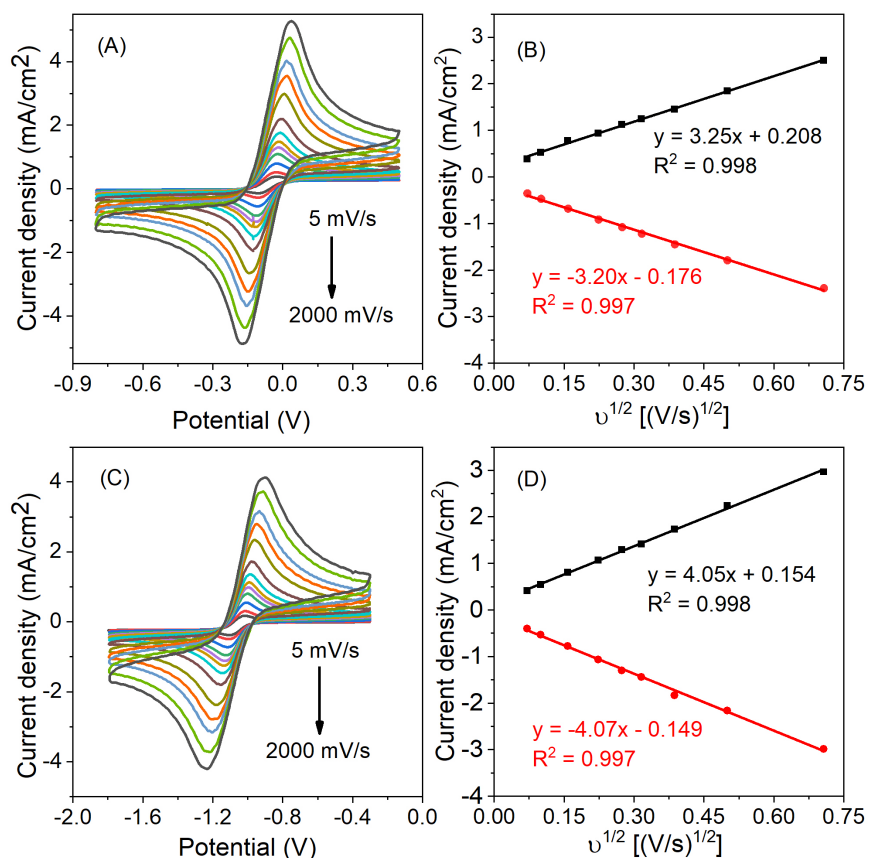


Figure S4. Cyclic voltammograms of 5.0 mM TCNE at scan rates from 5.0 to 2000 mV/s. (A) First reduction event. (C) Second reduction event. Fitting curve of CV peak current density and square root of scan rate for (B) the first and (D) the second redox process.

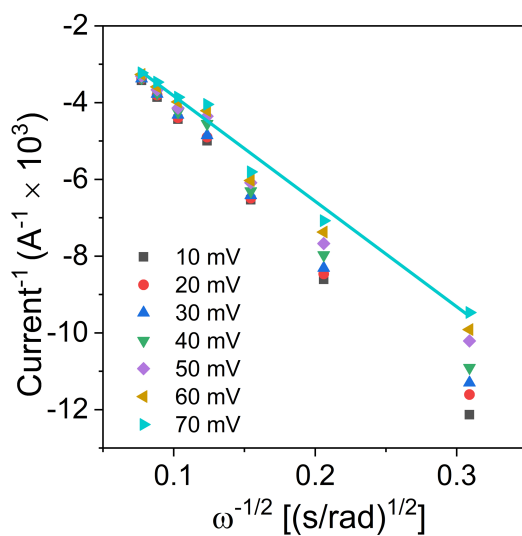


Figure S5. Koutecký-Levich curve (current⁻¹ vs. ω^{-1/2}) at different reduction overpotentials of the second reduction of TCNE.

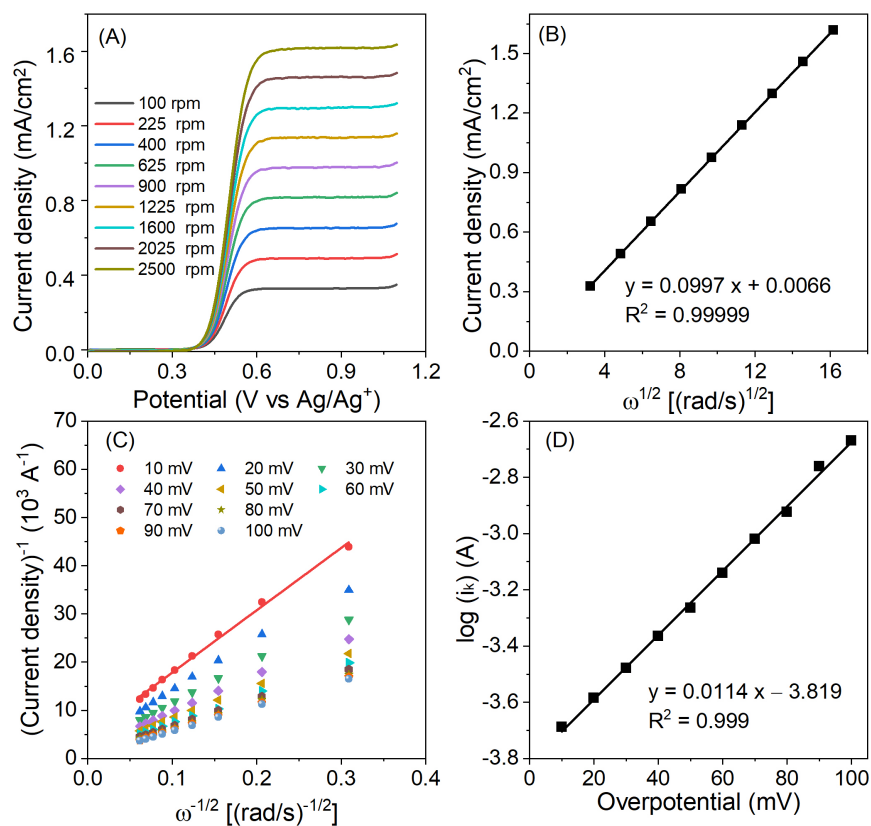


Figure S6. (A) Linear sweep voltammetry plots of **PEG1-PTZ** at different rotation rates of the rotating disk electrode. (B) Fitted linear Levich plots of the limiting current and square root of angular velocity. (C) Koutecký-Levich curve (current⁻¹ vs. $\omega^{-1/2}$) at different reduction overpotentials. (D) Tafel plot constructed using the current response and overpotentials. Solution: 1.0 mM **PEG1-PTZ** in 0.1 M NaClO₄/MeCN.

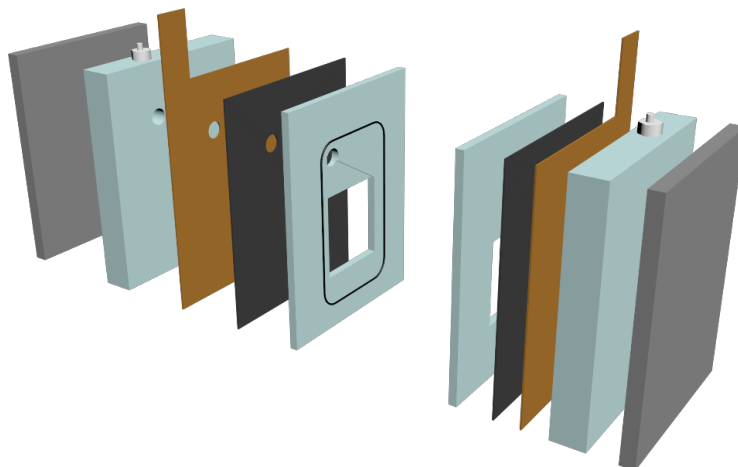


Figure S7. Schematic for static batteries.

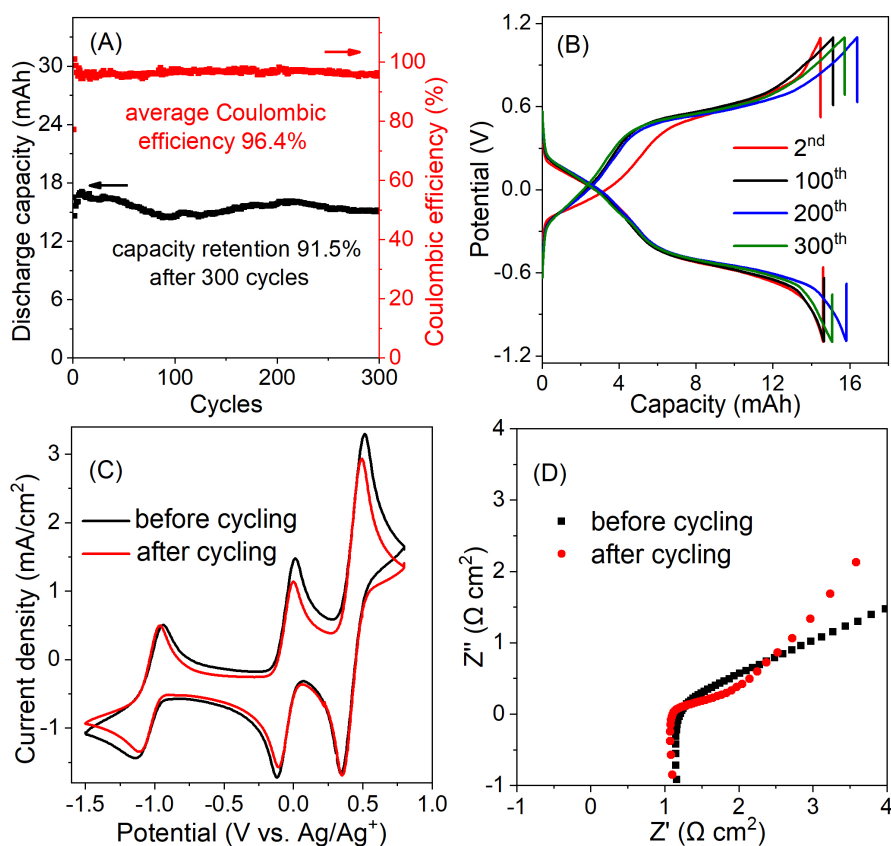


Figure S8. The 0.2 M-TCNE static battery. (A) Discharge capacity and Coulombic efficiency at 20 mA/cm². (B) Charge/discharge profiles at 2nd, 100th, 200th, and 300th cycles. (C) Cyclic voltammograms before and after cycling. (D) Nyquist impedance before and after cycling.

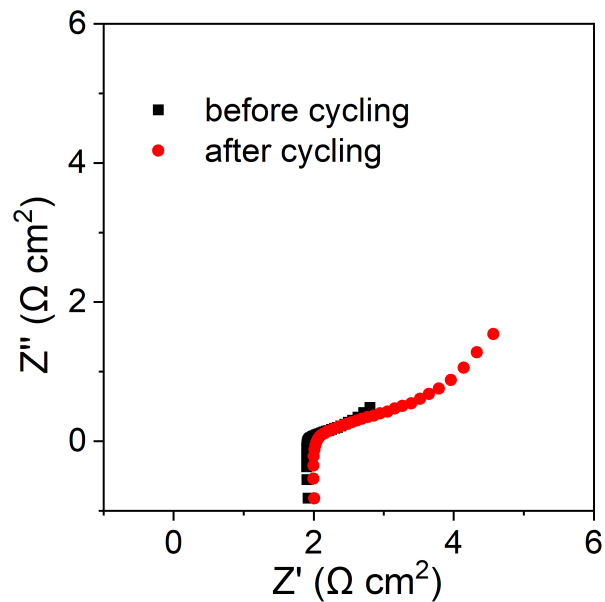


Figure S9. Nyquist impedance of the 0.5 M static TCNE/PEG1-PTZ battery before and after cycling.

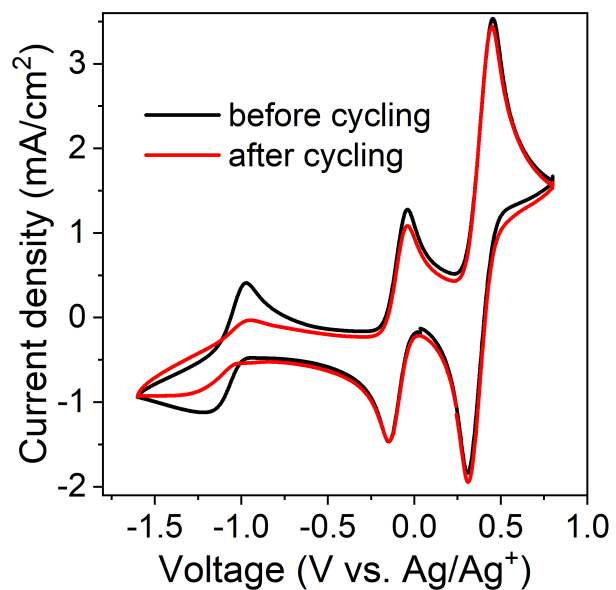


Figure S10. Cyclic voltammograms of the 0.2 M TCNE/PEG1-PTZ flow battery before and after cycling.

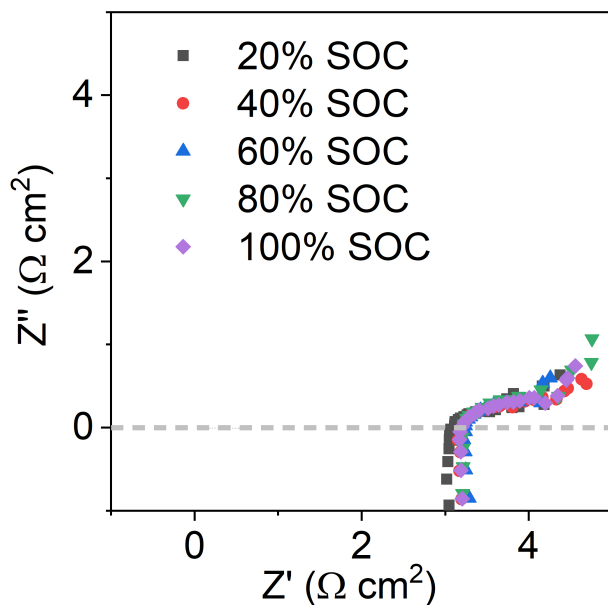


Figure S11. Nyquist impedance of the TCNE/PEG1-PTZ battery at 20%, 40%, 60%, 80% and 100% state-of-charge.

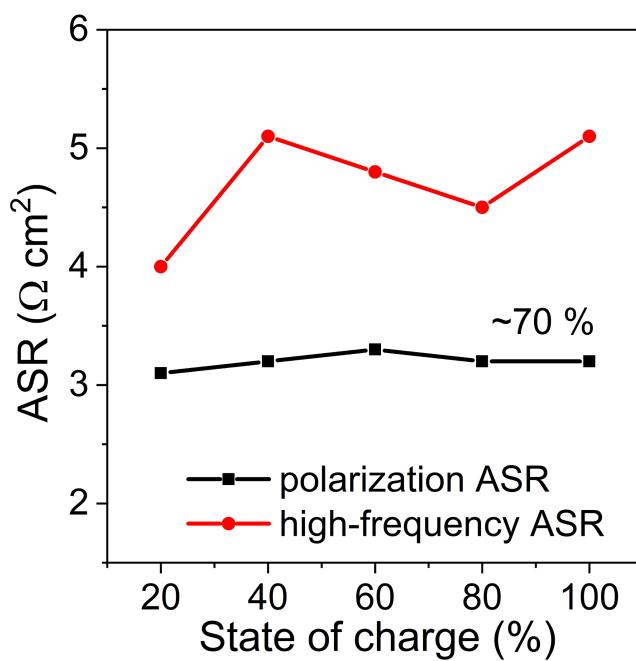


Figure S12. High-frequency ASR and polarization ASR of the battery vs. the state-of-charge.

Table S1. Performance parameters of reported organic RFBs.

Electrode materials	Concentration mol/L	Specific capacity Ah/L	Ref.
TCNE/PTZ	0.5	11.7	This work
ACA/Fe	0.5	20	S5
FMN/Fe	0.24	10	S6
DHPS/Fe	1.4	67	S7
MV/FcNCl	0.5	11.8	S8
MV/4-HOTEMPO	0.5	9.6	S9
FL/DBMMB	0.5	11.6	S10
MePh/DBMMB	0.3	6.2	S11
AB/DBMMB	1	46	S12

References

- S1. J. D. Milshtein, A. P. Kaur, M. D. Casselman, J. A. Kowalski, S. Modekrutti, P. L. Zhang, N. Harsha Attanayake, C. F. Elliott, S. R. Parkin, C. Risko, F. R. Brushett and S. A. Odom, *Energy Environ. Sci.*, 2016, **9**, 3531–3543.
- S2. J. Bachle, F. Goni and G. Grampp, *Phys. Chem. Chem. Phys.*, 2015, **17**, 27204–27029.
- S3. C. DeBruler, B. Hu, J. Moss, X. Liu, J. Luo, Y. Sun and T. L. Liu, *Chem*, 2017, **3**, 961–978.
- S4. M. J. T. Frisch, G. W.; Schlegel, H. B.; Scuseria, G. E.; Robb, M. A.; Cheeseman, J. R.; Scalmani, G.; Barone, V.; Petersson, G. A.; Nakatsuji, H.; Li, X.; Caricato, M.; Marenich, A.; Bloino, J.; Janesko, B. G.; Gomperts, R.; Mennucci, B.; Hratchian, H. P.; Ortiz, J. V.; Izmaylov, A. F.; Sonnenberg, J. L.; Williams-Young, D.; Ding, F.; Lipparini, F.; Egidi, F.; Goings, J.; Peng, B.; Petrone, A.; Henderson, T.; Ranasinghe, D.; Zakrzewski, V. G.; Gao, J.; Rega, N.; Zheng, G.; Liang, W.; Hada, M.; Ehara, M.; Toyota, K.; Fukuda, R.; Hasegawa, J.; Ishida, M.; Nakajima, T.; Honda, Y.; Kitao, O.; Nakai, H.; Vreven, T.; Throssell, K.; Montgomery, J. A.; Peralta, J. E.; Ogliaro, F.; Bearpark, M.; Heyd, J. J.; Brothers, E.; Kudin, K. N.; Staroverov, V. N.; Keith, T.; Kobayashi, J. Normand, K. Raghavachari, A. Rendell, J. C. Burant, S. S. Iyengar, J. Tomasi, M. Cossi, R.; Millam, J. M.; Klene, M.; Adamo, C.; Cammi, R.; Ochterski, J. W.; Martin, R. L.; Morokuma, K.; Farkas, O.; Foresman, J. B.; Fox, D. J. , *Wallingford CT*, 2016.
- S5. K. Lin, R. Gómez Bombarelli, E. S. Beh, L. Tong, Q. Chen, A. Valle, A. Aspuru-Guzik, M. J. Aziz and R. G. Gordon, *Nat. Energy*, 2016, **1**, 16102.
- S6. A. Orita, M. G. Verde, M. Sakai and Y. S. Meng, *Nat. Commun.*, 2016, **7**, 13230.
- S7. A. Hollas, X. Wei, V. Murugesan, Z. Nie, B. Li, D. Reed, J. Liu, V. Sprenkle and W. Wang, *Nat. Energy*, 2018, **3**, 508–514.
- S8. B. Hu, C. DeBruler, Z. Rhodes and T. L. Liu, *J. Am. Chem. Soc.*, 2017, **139**, 1207–1214.
- S9. T. Liu, X. Wei, Z. Nie, V. Sprenkle and W. Wang, *Adv. Energy Mater.*, 2016, **6**, 1501449.
- S10. X. Wei, W. Xu, J. Huang, L. Zhang, E. Walter, C. Lawrence, M. Vijayakumar, W. A. Henderson, T. Liu, L. Cosimbescu, B. Li, V. Sprenkle and W. Wang, *Angew. Chem. Int. Ed.*, 2015, **54**, 8684–8687.
- S11. X. Wei, W. Duan, J. Huang, L. Zhang, B. Li, D. Reed, W. Xu, V. Sprenkle and W. Wang, *ACS Energy Lett.*, 2016, **1**, 705–711.
- S12. L. Zhang, Y. Qian, R. Feng, Y. Ding, X. Zu, C. Zhang, X. Guo, W. Wang and G. Yu, *Nat. Commun.*, 2020, **11**, 3843.